Steel Innovations Conference 2013
Christchurch, New Zealand
21-22 February 2013

BUCKLING RESTRAINED BRACES: RESEARCH AND IMPLEMENTATION IN TAIWAN

K. C. Tsai[1], P. C. Lin[2], A. C. Wu[2], and M. C. Chuang[2]

ABSTRACT

The buckling-restrained brace (BRB) can be viewed as a high-efficiency energy dissipation device. It has been adopted for seismic buildings in Taiwan for decades. Several different types of BRB including the double-core BRB (DC-BRB) and the welded end-slot BRB (WES-BRB) have been investigated and implemented in building constructions. In this paper, the performance of the WES-BRB is illustrated through experimental tests of three full-scale components and a series of full-scale 3-story buckling-restrained braced frame (BRBF) tests applying large core strain exceeding 3.0%. For the BRBs, the unbonding material is one of the most important constituents. A method for estimating the compression strength adjustment factor considering the core plate Poisson and high model buckling effects for any given brace core strain is presented. In addition, the gusset plates in the BRBF can be subjected to the forces not only from the BRB but also from the frame action effects. In this study, the gusset interface force demands take into account the combined effect of the brace maximum axial force capacity and the peak beam shear possibly developed in the frame. An innovative cloud service named Brace On Demand (BOD) has been developed incorporating the seismic design procedures. User is only required to input the frame geometry and specify the BRB yield strength and type, then the BOD server instantaneously produces the detailed calculations for the WES-BRB, gusset dimensions, and welding details for downloading.

Introduction

The steel braced frame system can offer a cost-effective solution to meet the inter-story criterion on seismic buildings. Unlike the conventional braces could buckle in compression and lead to a sudden loss of stiffness and strength, the buckling restrained brace (BRB) can be viewed as a high-efficiency energy dissipation device through its development of full yield strength in both tension and compression in the BRB steel core (Fig. 1) (Watanabe et al. 1988). During the past decades, various BRB designs have been developed (Uang et. al 2004). The BRB steel core can be restrained by concrete or mortar filled in the steel encasing member (Watanabe et. al 1988, Iwata et. al 2000, Uang et. al 2004) or utilizing all steel construction (Uang et. al 2004, Eryaşar et. al 2010). In addition, it has been found that the BRB end-to-gusset connection is typically a bolted joint using several splice plates and two sets of bolts (Watanabe et. al 1988, Iwata et. al 2000) as shown in Fig. 2a, or like a double tee-to-gusset plate connection joint for the double-core BRB (DC-BRB) as shown in Fig. 2b (Tsai and Hsiao 2008). Recently, the development of the welded end-slot BRB (WES-BRB) (Lin et. al 2012) using the welded connection details can reduce the steel material usage and achieve a more compact cross section. On the other hand, to mitigate the friction developed between the steel core and the restrainer, the unbonding layers must be devised. The method for estimating the friction forces is proposed by the authors. The effectiveness of the unbonding layers in reducing the cyclic compressive and tensile strength difference is discussed in this paper. In order verify the performance of the WES-BRBs, several component and hybrid tests were conducted in the National Center for Research on Earthquake Engineering (NCREE) and National Taiwan University (NTU). The key features and the experimental performance of three full scale WES-BRBs and a series of 3-story large scale BRBF tests are presented. In addition, when the BRBF is deformed, the beam-to-column joint would either open or close. Thus, the corner gusset plate in the BRBF is required to sustain not only the BRB axial force but also additional forces resulted from the frame action

[1]Professor, Dept. of Civil Engineering, National Taiwan University, Taipei, 10617
[2] Assistant Researcher, National Center for Research on Earthquake Engineering, Taipei, 10668

(Kaneko et al. 2008, Chou et al. 2012). This paper introduces a simple seismic design method for the WES-BRB component and the gusset connections by incorporating the Generalized Uniform Force Method (GUFM) (Muir 2008) and the frame action forces computed from using the equivalent strut model (Lee 2002). The complete design procedures have been implemented by NCREE into a cloud web service "Brace On Demand" (BOD) to assist the designer to perform the automated design of BRBs and gusset connections through the use of internet.

Overview of BRB Research and Applications

The Double-core BRB

For the BRB-to-gusset connections, two major forms including butt-spliced (Watanabe et. al 1988, Iwata et. al 2000) and lap-spliced (Tsai and Hsiao 2008) connection details have been found common. Butt-spliced buckling-restrained brace (BS-BRB) is typically connected to the gusset plate by using several splice plates and two sets of bolts. Fig. 2a shows the BS-BRB with a cruciform cross section using eight splice plates. The DC-BRB is a typical lap-spliced BRB and has been developed (Lai and Tsai 2001) and extensively tested in NCREE and NTU. The DC-BRB is composed of two identical steel cores and restrainers as shown in Fig. 3. The two steel core plates are parallel to the gusset and the stiffeners are welded at the core end to increase the stability of the BRB ends. Thus, the DC-BRB members can be conveniently connected to the gusset plate by using either bolts (Fig 2b) or welding details. Compared with the BS-BRB, the DC-BRB using the lap-spliced connection details can reduce the connection segment length ($L_b/2$ in Fig. 2a and 2b) and increase the physical length of core segment to improve the fatigue life of the BRB (Watanabe et. al 1988). Furthermore, the welded BRB end connection details usually result in more compact joints than the bolted details. More than 11,000 sets of DC-BRBs have been manufactured and installed in about 60 buildings in Taiwan.

The WES-BRB

The welded BRB end connection can be cost-effective as it completely avoids the use of bolts and the connection plates. In addition, it can be found that the welded BRB connection details is more compact (Tsai and Hsiao 2008, Uang et al. 2004), and the connection length is significantly shorter than that required in the BRBs using bolted end connection details. This could improve the stability of the brace end outside the steel casing. Recently, the WES-BRB (Fig. 3b) have been developed and adopted in several test programs and new building constructions. In the WES-BRB connection (Figs. 3b and 4), the core plate is oriented perpendicular to the gusset and slotted at both ends. The brace axial force can go directly from one end of the core plate to the other end. In order to provide the stability of the BRB and its connections, a pair of offset stiffeners is welded to the core plate and gusset at each slotted end. If desired, these offset stiffeners can extend into the energy dissipation segment of the steel core to increase the BRB's axial stiffness and strength (Fig 4). The WES-BRBs have been adopted in the hybrid and cyclic loading tests of a 3-story single-bay full-scale BRBF (Lin et. al 2012) and several component tests ranging from small to extremely large load carrying capacities (Tsai et. al 2013). The tests confirm that the WES-BRBs and its welded connection details can effectively and stably dissipate energy. The number of WES-BRB applications in Taiwan building construction has been increasing in these years. A user-friendly cloud computing service for automated design of WES-BRBs and the gusset plate connections has been developed by NCREE. It will be discussed later.

Unbonding material and the strength adjustment factor

A typical BRB commonly consists of the core member, the buckling restrainer and the unbonding layer. When a properly designed and manufactured BRB is subjected to strain reversals, the differences between the cyclic peak compressive and tensile force responses should be as small as possible. The model seismic steel building provisions (AISC 2010) suggest that the compression strength adjustment factor $\boldsymbol{\beta}$ be less than 1.3 for each displacement excursion greater than the yield displacement. When the BRB is compressed, the core plate high mode buckling and the cross section expansion due to the Poisson effect are the two possible causes of a BRB to have the compressive strength higher than the tensile strength (Tsai et. al 2013).

When the BRB is subjected to a compression, lateral expansion enlarges the steel core area due to the Poisson effect. This is likely to increase the compressive axial force capacity. In addition, the space of the unbonding layer allows the steel core to buckle first in the weak-axis bending direction. Thus, the high mode buckling wave would form soon after the steel core deforms in the inelastic range. The wave crests of the core plate squeeze the unbonding material and produce the contact force on the buckling restrainer. As illustrated in Fig. 5, the contact force **N** can be estimated according to the geometric relationship between the

high mode buckling wave length $\mathbf{L_b}$ and the unbonding layer thickness **s**. The predicted compression strength adjustment factor **β** can be constructed from (Tsai et. al 2013):

$$\beta=\frac{1+\varepsilon}{1-\varepsilon}\left(1+\mu\frac{4s}{L_b}\right) \quad (1)$$

where **μ** is the friction coefficient between the steel core and the mortar. The core plate high mode buckling wave length $\mathbf{L_b}$ can be computed by adopting the equivalent flexural stiffness $\mathbf{(EI)_{eff}}$ of the core plate (Lin et. al 2012):

$$L_b=\sqrt{\frac{4\pi^2(EI)_{eff}}{P_{ysc}}}\approx 14t_p \quad (2)$$

where the $\mathbf{P_{ysc}}$ is the yield strength of the steel core. The high mode buckling wave length for the A572 GR50 steel is about 14 times the core thickness ($\mathbf{t_p}$). The Eq. 1 indicates that increase in the compressive strain **ε** or the unbonding layer thickness **s** would result in an increase of the **β** factor.

Experiments on WES-BRBs

Component tests

In order to verify the performance of the newly developed WES-BRB, three full-scale WES-BRB specimens were tested (Tsai et. al 2013). Specimen dimensions and cross-sectional profiles are shown in Table 1 and Fig. 6. All the core members of specimens were made of SN490B and covered with the chloroprene rubber as the unbonding layers. The steel rectangular and circular hollow sections served as the restrainer for Specimens WES-R and WES-C, respectively, were filled with the 56MPa mortar. The 12.5m long jumbo Specimen WES-J was made from encasing a core member using 48mm thick plates. The steel casing is a 610mm diameter, 12mm wall thickness STK400 pipe. The core is confined by infilling 56MPa self-compacting concrete. It is the longest and the strongest BRB specimen ever tested in Taiwan.

The 4900kN capacity universal testing load frame in NCREE was used for Specimens WES-R and WES-C (Figs. 7 and 8), while the 20000kN capacity universal testing load frame available at the Taiwan Architectural Building Research Institute was utilized for testing of Specimen WES-J (Fig. 9). The loading protocol followed the requirements of the AISC *Seismic provisions for structural steel buildings* (2010), except that additional 4 cycles of 2.75% and 2 cycles at 3.30% core strain (corresponding to $2.5\Delta_{bm}$ and $3.0\Delta_{bm}$, respectively) were applied for Specimen WES-R as listed in Table 2. Then the fatigue loading protocol, at the core strain corresponding to $1.5\Delta_{bm}$, continued until the core plate fractured.

The overall axial force versus deformation relationships for all specimens are given in Figs. 10 to 12. All specimens showed satisfactory performance with rather stable hysteretic response. The experimental maximum core strains were 3.30%, 3.00%, and 3.50% for Specimen WES-R, WES-C and WES-J, respectively. The core plates of Specimens WES-R, WES-C, and WES-J fractured at the 7th, 16th and 4th cycles, respectively, during the fatigue loading tests. The experimental compression strength adjustment value **β** (AISC 2010) was calculated for each strain level as tabulated in Table 3. It indicates that the maximum **β** values for Specimen WES-R, WES-C and WES-J are 1.18, 1.11 and 1.16, at the core strain levels of 3.30%, 3.00%, and 3.50%, respectively. The cumulative plastic deformation (CPD) values gained for these three specimens are 640, 834 and 406, respectively.

Full-scale hybrid tests

A series of hybrid and cyclic loading tests have been conducted on a 3-story single-bay full-scale BRBF (Lin et. al 2012). Six buckling-restrained braces (BRBs) including four WES-BRBs and two thin BRBs with welded end connection details were adopted in the BRBF specimen. Figs. 13a and 13b show the frame elevation of the BRBF specimen. The WES-BRBs were installed in the 2nd and 3rd story with circular and square (Fig. 4) steel casings, respectively, while the thin BRBs with rectangular steel casing (Fig.14) were installed in the 1st story. This BRBF was designed to sustain the design base earthquake (DBE) in Los Angeles. The fundamental vibration period of the BRBF is 0.603 second found from the numerical model and the design base shear force is 618kN. The LA03 ground accelerations with a peak ground acceleration (PGA) of 530gal was applied for two hybrid tests. The BRBs in the 1st story resist about 80% of the base shear and reach

about 90% of yield strength in both tension and compression under the design base shear force of 618kN.

During the first hybrid test, the inter-story drift reached about 0.03 radians for the 1st and 2nd stories and one of the thin BRB steel casing in the 1st story bulged out locally (Lin et. al 2012). The second hybrid test continued after the failed BRBs had been replaced with new BRBs using the thicker steel tubes. The following cyclic loading test stopped due to the fracture of one of the BRB core in the 1st story after the inter-story drifts reached about 0.03 radians for the 1st and 2nd story. The local bulging failure can be prevented by using proper steel casing design (Lin et al. 2012). The maximum experimental responses of the specimen are listed in Table 4. The CPD gained in each BRB in these tests are shown in Table 5. The maximum CPD of 817 is found in the south WES-BRB in the 2nd story.

During the three tests, more than 70% of the total hysteresis energy was absorbed by the BRBs in the 1st and 2nd stories in each test. And the energy absorbed by the specimen in the cyclic loading test was about four times of that in either hybrid test1 or test2. The test result shows that the WES-BRBs using the welded end connection details performed very well as it sustained the inter-story drift over 3.0% radian without failure.

Key Design Issues and Implementations

The BRB component design

As shown in Fig. 3, the BRB is primarily composed of a steel core, a buckling-restraint mechanism, and an unbonding mechanism. The steel core consists of three segments: a restrained yielding segment, a restrained non-yielding segment, and an unrestrained non-yielding segment (Fig. 6). Only the steel core is supposed to supply stiffness to the BRB. The effective stiffness of the BRB, $\mathbf{K_{eff}}$, can be calculated as follows (Tsai and Hsiao 2008):

$$K_{eff} = \frac{1}{\frac{L_c}{EA_c} + \frac{2L_t}{EA_t} + \frac{2L_j}{EA_j}} \tag{3}$$

where $\mathbf{L_c}$, $\mathbf{L_t}$, and $\mathbf{L_j}$ are the lengths of the restrained yielding, restrained non-yielding, and unrestrained non-yielding segments, respectively. $\mathbf{A_c}$, $\mathbf{A_t}$, and $\mathbf{A_j}$ are the cross-sectional areas of the restrained yielding, restrained non-yielding, and unrestrained non-yielding segments, respectively. The design of the BRBs' steel casing and the end connections must incorporate the maximum compressive strength $\mathbf{P_{max}}$ (AISC 2010):

$$P_{max} = \beta R_y P_{ysc} \tag{4}$$

where $\mathbf{R_y}$ is the steel core material overstrength factor. The Euler buckling strength $P_{cr} = \pi^2 E I_s / L_s^2$ is considered as the capacity of the steel casing (Tsai and Hsiao 2008), where $\mathbf{L_s}$ is the length of steel casing and $\mathbf{I_s}$ is the moment of inertia of the steel casing about the weak-axis bending.

The BRB connection design

As shown in Fig. 15, the corner gusset plates in the braced frame are subjected to additional tension or compression forces $\mathbf{P_{FA}}$ due to the opening and the closure of the corner adjacent to the beam-to-column joint when the frame deforms. As shown in Fig. 15a, the beam-to-column joint is opened when the BRB is compressed. In this case, the gusset plate is subjected to the compression due to the BRB compression force $\mathbf{P_{max,c}}$, and subjected to a tension force $\mathbf{P_{FA,t}}$ due to the opening of the beam-to-column joint. Likewise (Fig. 15b), when the beam-to-column joint is closed, the BRB is in tension. The gusset plate is subjected to the tension force from the BRB tension $\mathbf{P_{max,t}}$. In this case, the gusset is subjected to a compression $\mathbf{P_{FA,c}}$ due to the closure of the beam-to-column joint. A simple seismic design procedure for BRBF gusset plates is developed by incorporating the GUFM (Muir 2008) to compute the gusset interface forces result from the BRB axial force and the frame action forces computed from using the equivalent strut model (Lee 2002). The maximum force in the equivalent strut can be computed from the maximum beam shear $\mathbf{V_{beam}}$ as shown in Fig. 16. The maximum beam shear can be conservatively estimated from assuming the beam plastic hinges have formed adjacent to the gusset tip and column face (Figs. 15a and 15b). The horizontal (**S**) and vertical (**N**) force components (Fig. 16) of the strut axial force can be computed as follows (Lee 2002):

$$S=\frac{d_b L_h V_{beam}\left(0.3L-0.18L_h\right)}{4I_b/t_g+d_b L_h\left(0.3d_b+0.18L_v\right)} \text{ and } N=\frac{d_b L_v V_{beam}\left(0.3L-0.18L_h\right)}{4I_b/t_g+d_b L_h\left(0.3d_b+0.18L_v\right)} \quad (5)$$

where **L** is the beam clear length and $\mathbf{t_g}$ is the thickness of the gusset plate. Fig 17a shows the gusset interface forces when the BRB is in compression and beam-to-column joint opens. Fig 17b shows the BRB in tension with the closure of the beam-to-column joint. The shear force components result from the BRB and frame effects are always in the same direction. On the contrary, the normal forces on the interfaces due the two aforementioned effects are always in the opposite directions. The total force demands on the gusset interfaces can be computed by combining the BRB and frame actions together as follows:

$$\begin{aligned} H_c &= S-H_{uc} \quad V_c = N+V_{uc} \\ H_b &= S+H_{ub} \quad V_b = N-V_{ub} \end{aligned} \quad (6)$$

where $\mathbf{V_{uc}}$ and $\mathbf{H_{ub}}$ are the shear force demands, $\mathbf{H_{uc}}$ and $\mathbf{V_{ub}}$ are the normal force demands on the gusset interfaces induced by the BRB axial force computed by using the GUFM. According to the study (Lin et. al 2013), the gusset interface force demands can be satisfactory evaluated by the proposed method. These force demands can be adopted for several gusset design limit states including the von Mises yield criteria, and tension and shear rupture failure near the gusset interface.

The cloud service BOD for the design of the WES-BRBs and gusset connections

The complete procedures for the seismic design of the WES-BRBs and corresponding gusset connections have been documented and implemented into a cloud service by NCREE to assist the practitioners in conducting BRBF design (Chuang et. al 2012). This cloud service (http://BOD.ncree.org.tw) is named as Brace On Demand (BOD). The BOD provides the on-demand service for users to find the WES-BRBs and corresponding connection details that meet their design requirements. It checks all design limit states, reports all the demand to capacity ratio, and output the final design. User is only required to input the frame geometry, specify the BRB yield strength and steel grade in the BOD Browser (Fig. 18), then the BOD server can instantaneously produce the calculations including the detailed profiles of WES-BRB, gusset dimensions and welding details for downloading. The results computed by BOD can be archived for download in two formats (.txt and .xls). Thus, the BOD is an effective tool for structural engineers and steel fabricators engaged in the building projects using WES-BRBs.

Conclusions

1. A method of considering the Poisson and high mode buckling effects into the prediction of the compression strength adjustment **β** factor is proposed. From the experimental results, it appears that the compression strength adjustment factor can be reasonably predicted for a well made BRB.
2. The high mode buckling wave length of the BRB core can be estimated by incorporating the equivalent flexural stiffness $\mathbf{(EI)_{eff}}$ of the steel core into the Euler buckling equation. For A572 GR50 steel, the wave length is about 14 times of the core plate thickness computed from the proposed method and observed from the experiments.
3. The fabrication of the WES-BRB is cost-effective and its connection is very compact which could increase the BRB energy dissipation segment. The experimental compression strength adjustment factors **β** resulted from very large strain cycles are all less than 1.2 based on the test results of three full-scale component tests. The excellent performance of the WES-BRBs is confirmed with a very stable hysteretic response and very good capability in achieving a CPD value greater than 400 times the yield deformation.
4. Throughout the 3-story BRBF hybrid tests, the WES-BRB specimens in the 2^{nd} story remained intact after the frame specimen was imposed to a large inter-story drift greater than 0.03 radians. The WES-BRB sustained a peak core strain of about 4%, and gained a CPD greater than 800.
5. In the BRBF, the gusset interface forces resulted from the BRB and frame actions are combined to compute the force demands on gusset plate. The seismic design procedures incorporate the GUFM and the equivalent strut model. The peak axial force in the equivalent strut can be estimated from a beam shear force corresponding to the beam plastic hinge forms at the gusset tip.
6. The Brace On Demand (BOD) has been developed as an aid for structural engineers in practicing BRBF design. This cloud service greatly improves the productivity of engineers in conducting the seismic building design using the WES-BRBs. A number of applications have confirmed that the BOD is effective for users engage in seismic research and practice. The BOD browser can be downloaded for free from the website (http://bod.ncree.org.tw).

Acknowledgements

The financial and technical supports provided by the Taiwan National Science Council and National Center for Research on Earthquake Engineering are very much appreciated.

References

AISC, 2010. Seismic provisions for structural steel buildings, *American Institute of Steel Construction, Inc*., Chicago, Illinois.

Chou, C.C., Liu, C.H., and Pham, D.H., 2012. Steel buckling-restrained braced frames with single and dual corner gusset connections: seismic tests and analysis, *Earthquake Engineering and Structural Dynamics*, 41(7), 1137-1156.

Chuang. M.C., Tsai. K.C., Lin, P.C., and Wu, A.C., 2012. A cloud service for seismic design of buckling restrained braces and connections, *Proceedings of the 25th KKCNN Symposium on Civil Engineering*, Busan, Korea.

Eryaşar, M.E. and Topkaya, C., 2010. An experimental study on steel-encased buckling-restrained brace hysteretic dampers, *Earthquake Engineering and Structural Dynamics*, 39, 561-581.

Iwata, M., Kato, T., and Wada, A., 2000. Buckling-restrained braces as hysteretic dampers. *Behaviour of Steel Structures in Seismic Areas*. Balkema: Rotterdam; 33-38.

Kaneko, K., Kasai, K., Motoyui, S., Sueoka, T., Azuma, Y., and Ooki, Y., 2008. Analysis of beam-column-gusset components in 5-Story value-added frame, *Proceedings of the 14th world conference on Earthquake Engineering*, Beijing, China.

Lai, J.W. and Tsai, K.C., 2001. A study of buckling restrained brace frames, Center for Earthquake Engineering Research *Report No. CEER/R90-07*, National Taiwan University. (in Chinese)

Lee, C.H., 2002. Seismic design of rib-reinforced steel moment connections based on equivalent strut model, *Journal of Structural Engineering,* 1121-1129.

Lin, P.C., Tsai, K.C., Wu, A.C., and Chuang, M.C., 2013. Seismic design and test of gusset connections for buckling-restrained braced frames, *Earthquake Engineering and Structural Dynamics,* (in review)

Lin, P.C., Tsai, K.C., Wang, K.J., Yu, Y.J., Wei, C.Y., Wu, A.C., Tsai, C.Y., Lin, C.H., Chen, J.C., Schellenberg, A.H., Mahin, S.A. and Roeder, C.W., 2012. Seismic design and hybrid tests of a full-scale three-story buckling-restrained braced frame using welded end connections and thin profile, *Earthquake Engineering and Structural Dynamics*, 41(5), 1001-1020.

Muir, L.S., 2008. Design compact gussets with the uniform force method, *Engineering Journal*, 1st quarter.

Tsai, K.C. and Hsiao, P.C., 2008. Pseudo-dynamic tests of a full-scale CFT/BRB frame-Part II: Seismic performance of buckling-restrained braces and connections, *Earthquake Engineering and Structural Dynamics,* 37 (7), 1099-1115.

Tsai, K.C., Wu, A.C., Wei, C.Y., Lin, P.C., and Chuang, M.C., 2013. Unbonding layers and welded end-slot connection for buckling-restrained braces, *Earthquake Engineering and Structural Dynamics*, (in review)

Uang, C.M., Nakashima, M., and Tsai, K.C., 2004. Research and application of buckling-restrained braced frames, *Steel Structures* 4, 301-313.

Watanabe, A., Hitomi, Y., Saeki, E., Wada, A., and Fujimoto, M., 1988. Properties of braces encased in buckling-restraining concrete and steel tube. *Proceedings of the 9th World Conference on Earthquake Engineering,* Tokyo-Kyoto, Japan, 4, 719-724.

Wu, A.C., Lin, P.C., and Tsai, K.C., 2013. High mode buckling responses of buckling-restrained brace core plates, *Earthquake Engineering and Structural Dynamics,* (in review)

Table 1. Dimensions for WES-BRB specimens

Specimen	F_y (MPa)	A_c (mm^2)	L_c (mm)	L_t (mm)	L_j (mm)	L_{BRB} (mm)	Steel casing (mm)
WES-R	334	4000	1700	200	200	2500	Tube 175×175×4.5
WES-C	388	7525	2060	100	520	3300	Pipe 267.4×6
WES-J	400	26500	9500	286	1214	12500	Pipe 609.6×12

Table 2. Core strain at each deformation level for WES-BRB specimens

Specimen	Core strains at various deformation targets						
	Standard				Extra		Fatigue
	$0.5\Delta_{bm}$	$1.0\Delta_{bm}$	$1.5\Delta_{bm}$	$2.0\Delta_{bm}$	$2.5\Delta_{bm}$	$3.0\Delta_{bm}$	$1.5\Delta_{bm}$
WES-R	0.55%	1.10%	1.65%	2.20%	2.75%	3.30%	1.65%
WES-C	0.75%	1.50%	2.25%	3.00%	-	-	2.25%
WES-J	0.88%	1.75%	2.63%	3.50%	-	-	2.63%

Table 3. Experimental compression strength adjustment **β** and CPD values for WES-BRB specimens

Specimen	Experimental β_E values at various deformation targets						CPD
	$0.5\Delta_{bm}$	$1.0\Delta_{bm}$	$1.5\Delta_{bm}$	$2.0\Delta_{bm}$	$2.5\Delta_{bm}$	$3.0\Delta_{bm}$	
WES-R	1.13 1.14	1.13 1.15	1.14 1.15	1.14 1.14	1.16 1.18 1.17 1.16	1.18 1.18	640
WES-C	1.02 1.06	1.06 1.08	1.09 1.09	1.11 1.11	-	-	834
WES-J	1.01 1.07	1.07 1.07	1.11 1.11	1.16 1.15	-	-	406

Table 4. The maximum responses of the BRBF in the hybrid test1, test2, and cyclic loading test

	hybrid test1		hybrid test2		cyclic loading test	
	inter-story drift (radian)	story shear (kN)	inter-story drift (radian)	story shear (kN)	inter-story drift (radian)	story shear (kN)
3rd story	0.0095	1036	0.0089	1067	0.0090	967
2nd story	0.0293	1605	0.0327	1701	0.0310	1656
1st story	0.0283	2134	0.0280	2207	0.0320	1967

Table 5. BRB specimens CPD gained in the hybrid test1, test2, and cyclic loading test

	hybrid test1	hybrid test2	cyclic loading test	Total
3BRB_N	40	39	109	188
3BRB_S	44	41	72	157
2BRB_N	149	132	524	805
2BRB_S	172	137	508	817
1BRB_1N	220	-	-	220
1BRB_1S	128	-	-	128
1BRB_2N	-	166	500	666
1BRB_2S	-	173	512	685

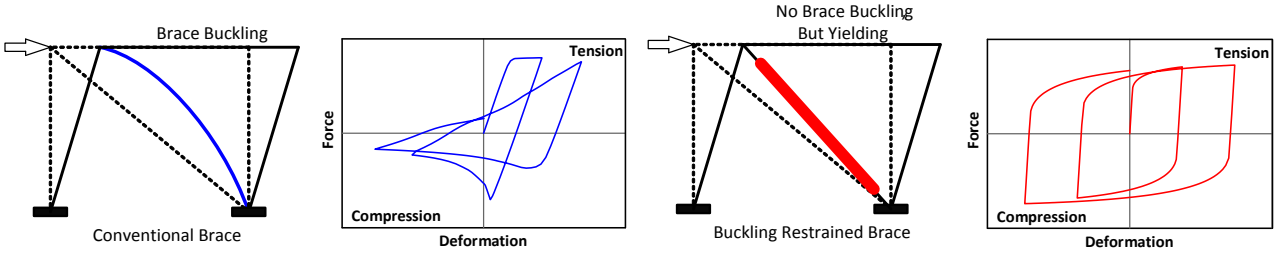

Figure 1. The forces versus deformation relationships of buckling and buckling-restrained braces.

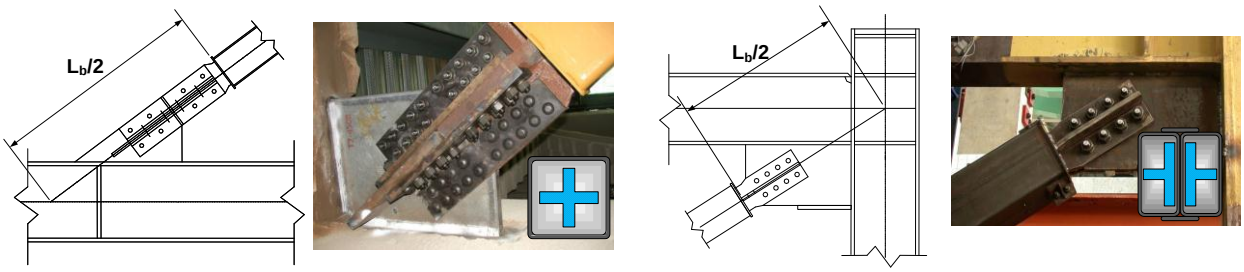

Figure 2. The BRB end-to-gusset connection configurations of (a) the BS-BRB and (b) the DC-BRB.

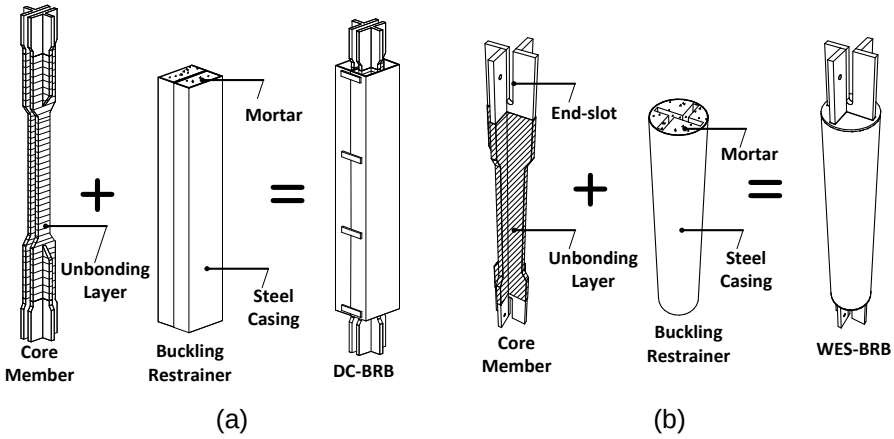

Figure 3. Schematic of the compositions of (a) the DC-BRB and (b) the WES-BRB.

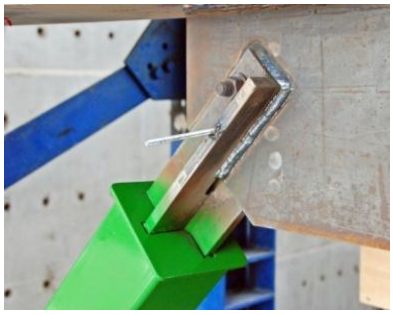

Figure 4. The WES-BRB to gusset connection details.

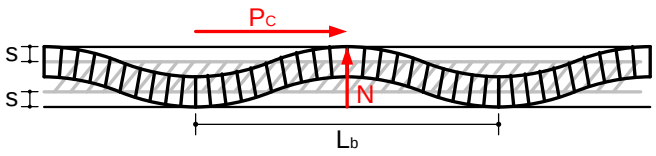

Figure 5. Schematic of the high mode buckled brace core.

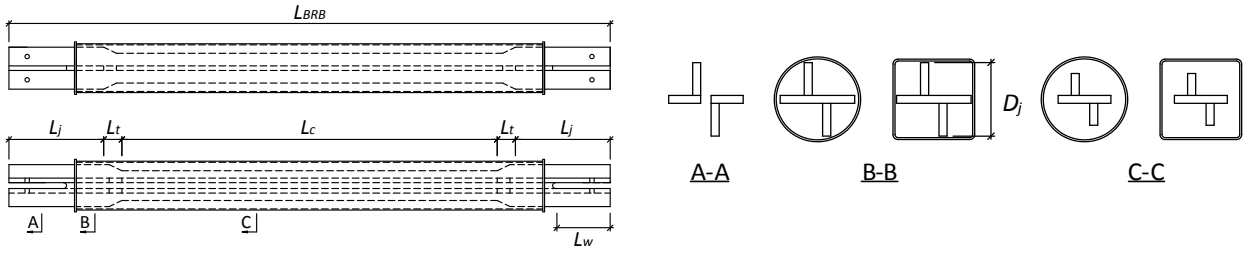

Figure 6. Profiles and cross sections of the WES-BRB component test specimen.

Figure 7. Test setup for WES-R.

Figure 8. Test setup for WES-C.

Figure 9. Test setup for WES-J.

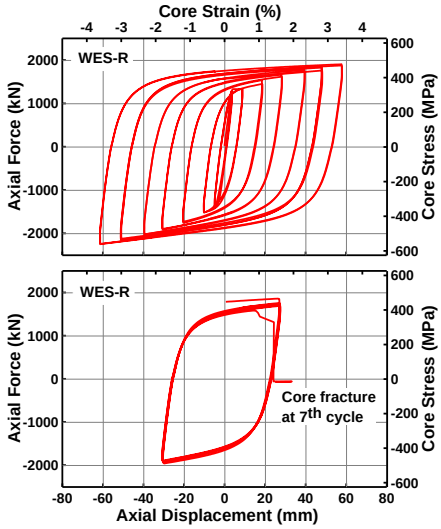

Figure 10. Responses of WES-R.

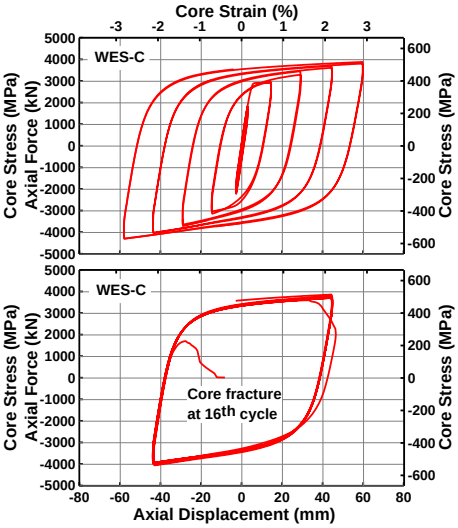

Figure 11. Responses of WES-C.

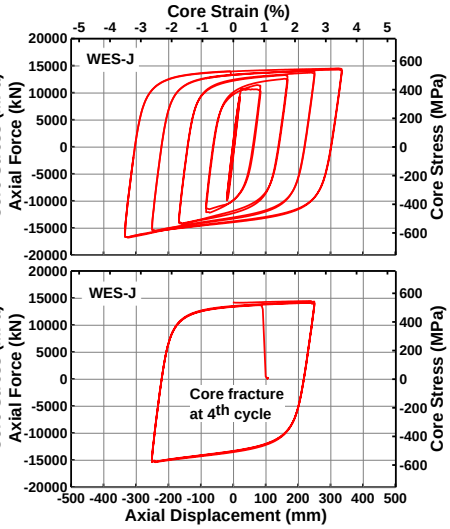

Figure 12. Responses of WES-J.

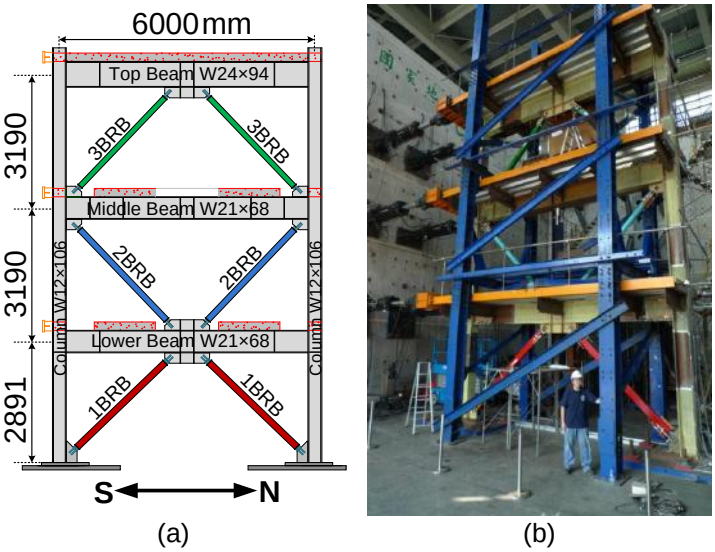

Figure 13. (a) The BRBF elevation, (b) the BRBF test setup.

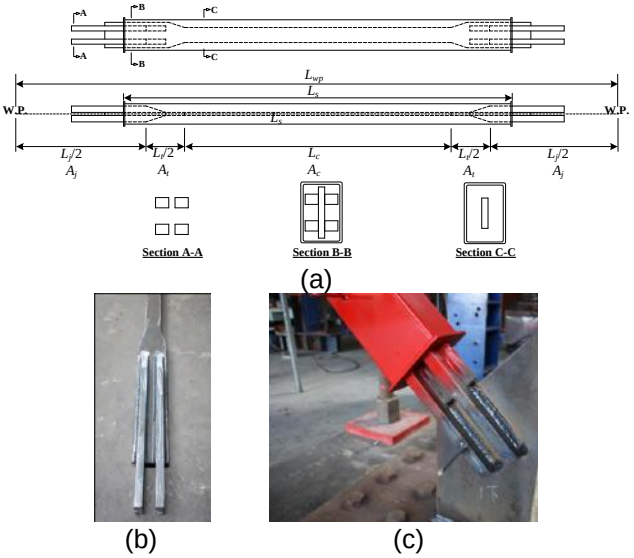

Figure 14. The profiles of (a) thin BRB and its (b) core steel using (c) welded connection.

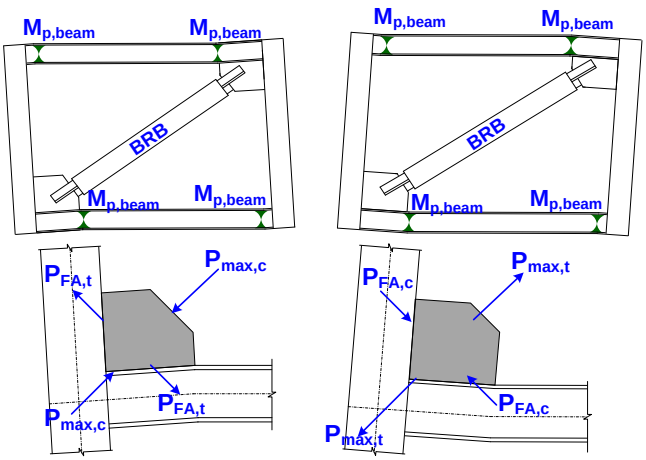

Figure 15. The forces acting on gusset plate under the frame action effects.

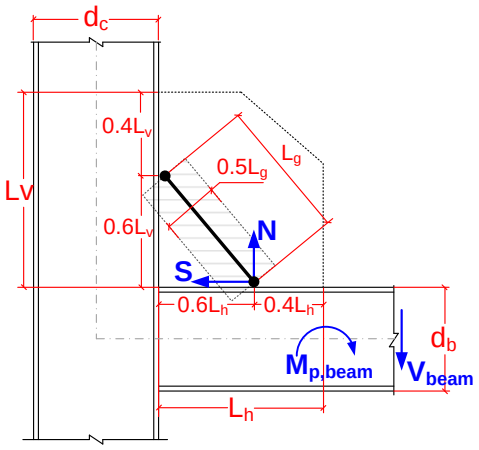

Figure 16. The equivalent strut model for the frame action effect.

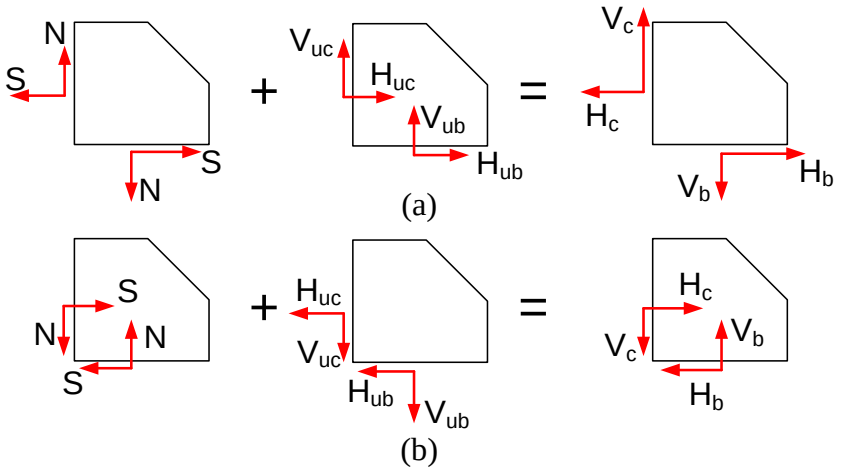

Figure 17. Combinations of the BRB and frame action forces.

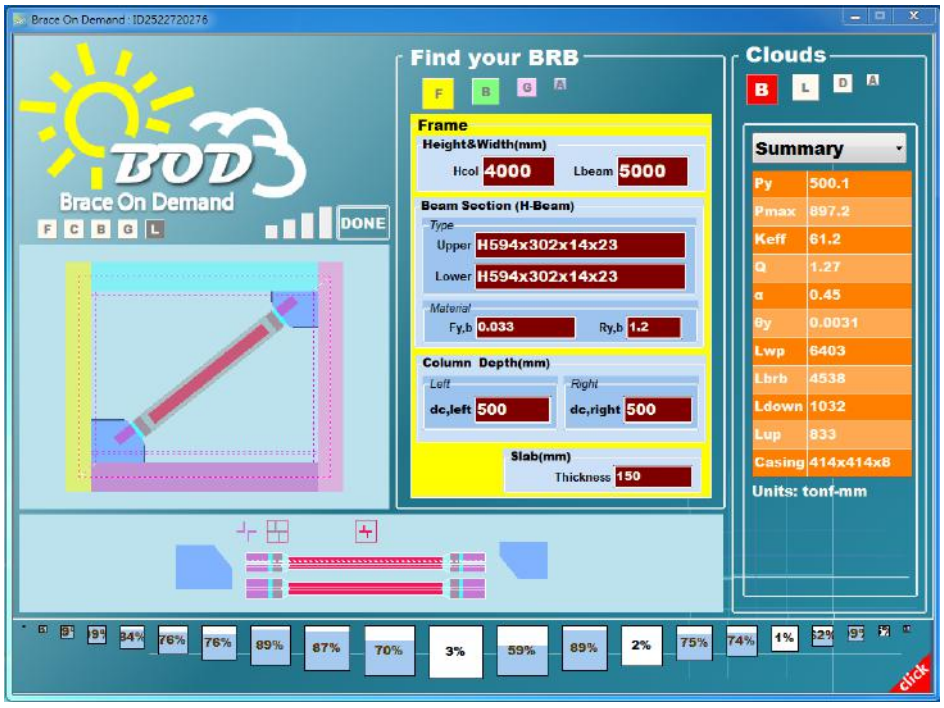

Figure 18. The BOD Browser.